High-rate deformation and fracture under extreme conditions

V.E. Fortov, G.I. Kanel

Joint Institute for High Temperatures of Russian Academy of Sciences, Izhorskaya 13, bld. 2,

Moscow, 125412 Russia

fortov@ihed.ras.ru, kanel@ficp.ac.ru

Keywords: shock waves, high strain rates, inelastic deformation, fracture, polymorphic transformations

Abstract. The shock-wave techniques present a powerful tool for studying the properties of materials at extremely high strain rates with well-controllable loading conditions. The paper presents our latest results of investigations of inelastic deformation and fracture of solids in different structural states under conditions of shock-wave loading. The time range available for shock-wave measurements has been recently expanded to picoseconds and approaching the ultimate tensile and shear strength values becomes real that allows approaching the ultimate ("ideal") shear and tensile strength of solids. Results of measurements are transformed into dependences of plastic strain rate on the shear stress and the damage rate on the stress. The impact loading of a glass and, probably, other brittle materials can result in the appearance of a failure wave. The failure wave is a network of cracks that are nucleated on the surface and propagate into the elastically stressed body. It is a mode of catastrophic fracture in an elastically stressed media whose relevance is not limited to impact events. The shock-wave response of sapphire is characterized by high heterogeneity of deformation for some orientations. As a result of inelastic deformation, sapphire looses its tensile strength which is very high within the elastic domain.

Introduction

The shock-wave techniques present a powerful tool for studying the properties of materials at extremely high strain rates with well-controllable loading conditions. Progress in investigations into high-rate deformation, fracture, and physico-chemical transformations in shock waves has been provided by the development of techniques for measuring wave profiles with a high spatial and temporal resolution. Modern methods for the recording of pressure and particle velocity histories made it possible to take into consideration the structural details of compression and rarefaction waves and their evolution, thereby making available the information about a material response to intense dynamic loads. At the present time there exists extensive experimental information on the elastic-plastic and strength properties of technical metals and alloys, geological materials, ceramics, glasses, polymers and elastomers, ductile and brittle single crystals in the microsecond and nanosecond time ranges. The time range available for shock-wave measurements has been recently expanded to picoseconds and approaching the ultimate tensile and shear strength values becomes real. The experimental data form the basis for developing constitutive equations and models of high-rate inelastic deformation and fracturing, as well as macrokinetic models of physico-chemical transformations, which are required to calculate explosions, high-speed impacts, and the interaction of high-power radiation pulses with matter.

Rate and temperature effects on the flow stress and tensile strength of metals and alloys

It is well known that the flow stress of crystalline solids increases with an increase in the strain rate. For many metals, this dependence sharply increases, when the rate of deformation exceeds ~10^3–10^4

s^{-1}, which is interpreted as the consequence of the change in a mechanism of dislocations motion [1, 2]. For small strain rates, dislocation overcomes obstacles due to the joint action of the applied stress and thermal fluctuations. Because of this, the increase of temperature is accompanied by the decrease in the yield strength of materials. For sufficiently high strain rates, the dominant drag mechanism becomes the phonon viscosity. Because the phonon viscosity is proportional to the temperature, for very high strain rates one can expect an increase in the flow stress with an increase in temperature [3] as it is shown in Fig. 1.

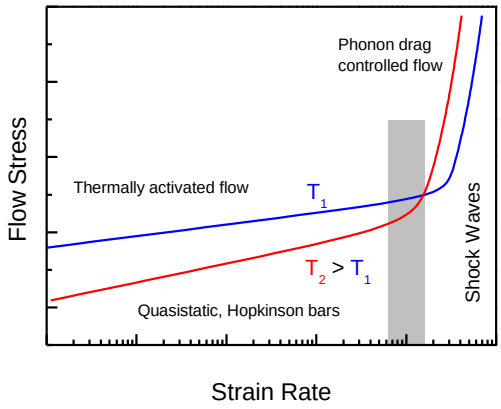

Figure 1. General time–temperature dependences of the yield stress.

Investigations of temperature-rate relations of the resistance to deformation and fracture of metals and alloys at shock-wave loading are motivated by the need in a basis for developing the models and constitutive relationships which would be workable over wide range of strain rates, stresses and temperatures, search for new information about basic mechanisms and governing factors of these processes, and by necessity to provide experimental basis for atomistic simulations of the deformation and fracture processes. Main methods of studying elastic-plastic and strength properties of shocked solids are well developed [4-11]. There are two direct (without computer simulations) ways to get information about relationships between the plastic strain rate and the flow stress: measurements of the decay of the elastic precursor wave [4, 5] and measurements of the rise time of plastic shock wave [6, 7]. The high-rate fracture is studied by means of analyzing the spall phenomena [10, 11]. The time range available for shock-wave measurements has been recently expanded to picoseconds [12, 13] and approaching the ultimate tensile and shear strength values becomes real. In this paper, we try to summarize and analyze last experimental data on high-rate plastic deformation and fracture of metals and alloys.

Precursor decay and initial plastic strain rate

Decay of the elastic precursor is caused by the stress relaxation behind its front and is connected with plastic strain rate $\dot{\gamma}_p = (\dot{\varepsilon}_x^p - \dot{\varepsilon}_y^p)/2$ by the relation [4, 5]:

$$\left.\frac{d\sigma_x}{dh}\right|_{\mathrm{HEL}} = -\frac{4}{3}\frac{G\dot{\gamma}_p}{c_l} \qquad (1)$$

where h is the propagation distance, G is the shear modulus and c_l is the precursor wave velocity which is equal to the longitudinal sound speed. Figure 2 summarizes experimental data [12-18] for aluminum. The HEL value from 50 MPa at 10 mm up to 20.5 GPa at 1.2 μm of the propagation

distance. It is interesting to note that 20.5 GPa of elastic stress is realized also inside steady shock wave in aluminum which propagates with the same speed U_S = 7.8 km/s at 38.7 GPa of the peak stress. Such large compression causes significant increase of the shear modulus in (1). Solid points in Fig. 2 present normalized values $\sigma_{HEL}G_0/G$ [14]. With this correction the whole set of data in Fig. 1 is reasonably described by empirical relationship

$$\sigma_{HEL} = S(h/h_0)^{-\alpha} \qquad (2)$$

with h_0 = 1 mm, S = 0.16 GPa, and the exponent α = 0.63. The value of maximum shear stress at the HEL is

$$\tau_{HEL} = (3/4)\sigma_{HEL}\left(1 - c_b^2/c_l^2\right) = \sigma_{HEL}\, G/E', \qquad (3)$$

where $E' = \rho_0 c_l^2$ is the longitudinal elastic modulus. With obtained empirical relationship (2) we finally obtain from (1) the initial plastic strain rate as a function of shear stress:

$$\dot{\gamma}_p = \frac{3}{4}\left(\frac{\tau\ E'}{SG}\right)^{\frac{\alpha+1}{\alpha}} \frac{S\alpha c_l}{h_0 G} \quad \text{or} \quad \dot{\gamma}_p = 9.1\times10^7\left(\tau/\tau_0\right)^{2.59}\ \text{s}^{-1}$$

where τ_0 = 1 GPa. The plastic strain rate decreases from 10^9 s^{-1} at 1 μm of the propagation distance to 10^3 s^{-1} at 5-10 mm. At this distance, the decay of HEL sharply decelerates. At ~(2-5)×10^3 s^{-1} the Hopkinson bar tests show sharp increase of sensitivity of the flow stress to the strain rate [19].

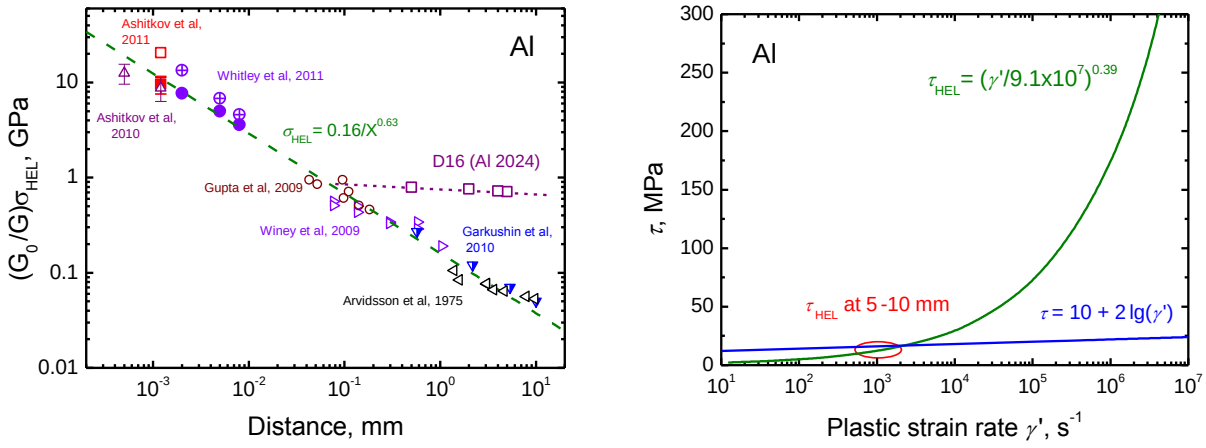

Figure 2. Decay of the elastic shock wave in aluminum. Solid points present corrected data. The HEL data for pure and technical aluminum from [12-18] are presented. For comparison, parameters of the elastic precursor wave in D16 aluminum alloy (Al 2024 in USA) are shown.

Figure 3. Rate sensitivity of the flow stress in aluminum.

Figure 3 compares low-rate [1, 19] and high-rate branches of total flow stress dependence on the strain rate for aluminum. It may be expected that for harder aluminum alloys the low-rate branch should intersect the high-rate branch at higher stress and higher strain rate.

As it can be seen in Fig. 4, D16 aluminum alloy (Al 2024 in USA) exhibits very weak decay of the elastic precursor wave between 0.5 mm and 5 mm of the propagation distance. In this range of distances, the Hugoniot elastic limit of the alloy is around 0.71 GPa. In aluminum such HEL is realized at 92 μm where the plastic strain rate is ~7×10^5 s^{-1}. It is natural to suppose that at smaller sample thicknesses the behavior of the D16 alloy does not so much differ from aluminum. The decay of precursor wave in Ma2-1 magnesium alloy [17] between 0.25 mm and 10 mm is stronger than that in D16 but weaker than that in aluminum: $\sigma_{HEL} = 0.483(h/h_0)^{-0.315}$ GPa. Probably faster decay occurs at $h < 0.25$ mm.

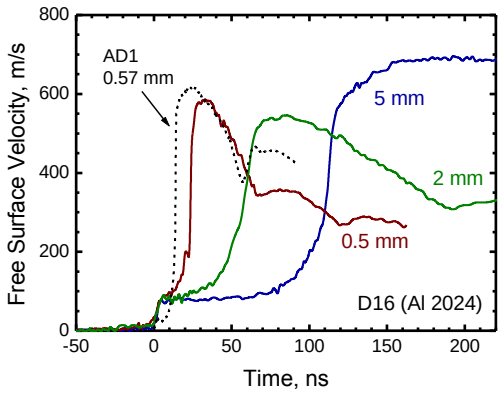

Figure 4. Free surface velocity histories of D16 aluminum alloy samples of various thicknesses. An AD1 aluminum is presented for comparison.

Hardening of a material by decreasing grain size or by other method may appear or not appear in increase of the HEL value depending on the branch of the $\tau(\dot{\gamma}_p)$ dependence which is realized for chosen sample thickness [20]. Moreover, it was observed [21] that harder ultra-fine-grained tantalum may demonstrate even lower HEL value than less hard coarse-grained one. Probably it is explained by faster decay in the ultra-fine-grained material where grain boundaries may be the dislocation sources.

In regard of dislocation mechanisms of high-rate plastic deformation, it follows from atomistic simulations [22, 23] the dislocation speed in aluminum at room temperature linearly grows with increasing shear stress up to ~100 MPa; after which the velocity grows abruptly slackens. If to assume the plastic strain rate is controlled by velocity of dislocations, we should have linear or weaker dependence $\dot{\gamma}_p(\tau)$. Since experiments give much stronger dependence even for initial strain rate, we should suppose that the process is controlled by the rate of nucleation or generation of dislocations rather than by their speeds.

Strain rate in plastic shock wave

The shear strain rate at uniaxial shock compression is:

$$\dot{\gamma} = \dot{\varepsilon}_x/2 = \dot{\gamma}_e + \dot{\gamma}_p = \dot{\tau}/G + \dot{\gamma}_p \qquad (4)$$

where $\dot{\varepsilon}_x$ is the total strain rate which is determined from measurements of the rise time and $\dot{\gamma}_e$ is the elastic shear strain rate. The shear stress in plastic shock wave passes through a maximum. In the point of maximum $\dot{\tau} = 0$ and $\dot{\gamma}_p = \dot{\varepsilon}_x / 2$. Corresponding shear stress is estimated from maximum difference between the stress σ_x on the Rayleigh line and the pressure p on the Hugoniot of material at the same total strain [6, 7].

Comparison of the data presented in Fig. 5 shows that the plastic strain rate in shock wave is larger by order of magnitude than that at the top of elastic precursor wave at the same shear stress. Acceleration of plastic deformation is obviously a result of multiplication of dislocations.

Temperature effects

Some metals and ion crystals demonstrate anomalous growth of the Hugoniot elastic limit with heating. Figure 6 presents an example of the free surface velocity history of aluminum sample measured at elevated temperature in comparison with the room temperature data at the same impact conditions [17]. The increase in temperature has lead to a significant increase in the amplitude of elastic precursor and the increase in the rise time of the plastic shock wave from 3-5 ns up to 8–12 ns. In part, the increase of HEL is caused by the decrease in the longitudinal sound velocity with heating that appears also in decreased time interval between elastic and plastic waves in Fig. 6.

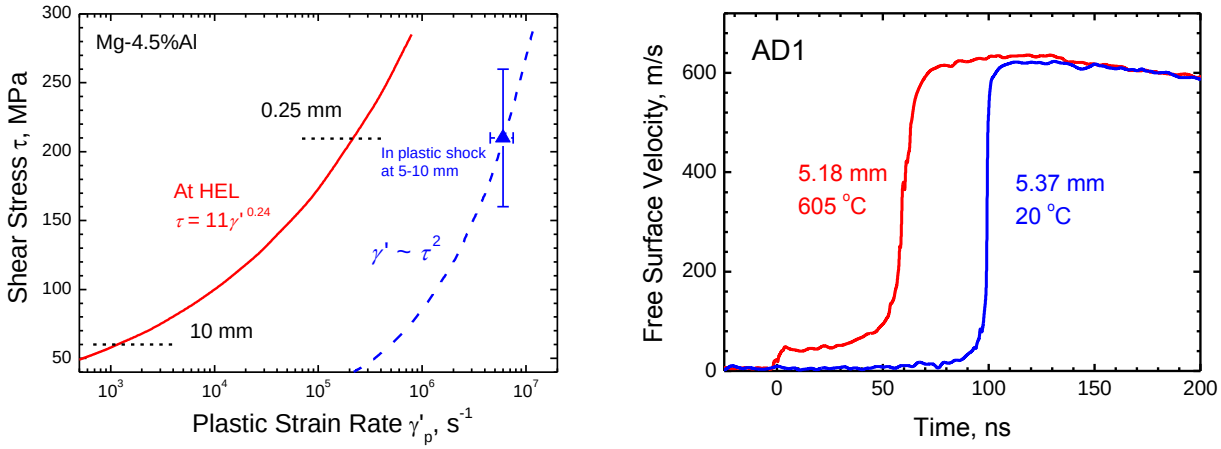

Figure 5. Relationship between the plastic strain rate and shear stresses behind the elastic precursor front (line) and in plastic shock wave (point) at shock compression of Ma2-1 magnesium alloy [24].

Figure 6. Free surface velocity histories of AD1 aluminum plates at room temperature and 605°C

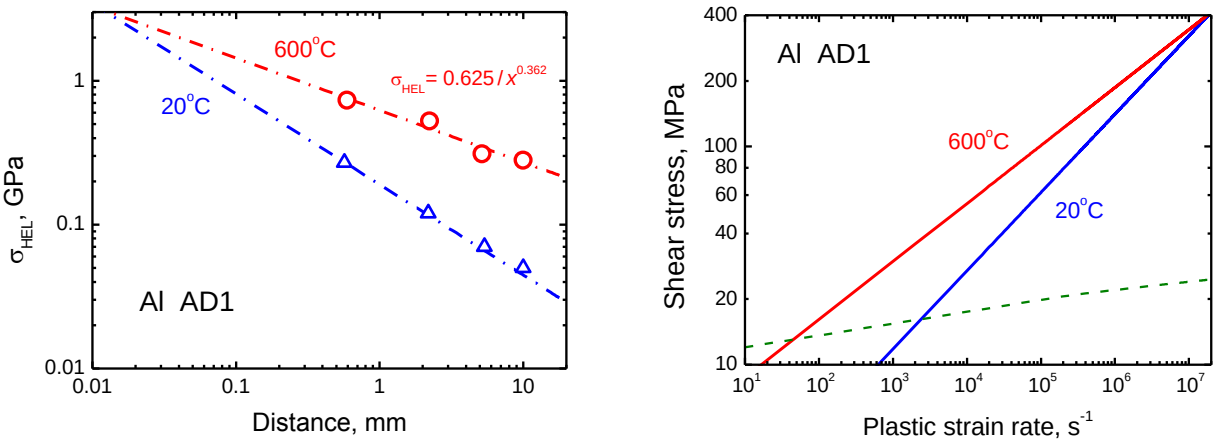

Figure 7. Decay of elastic precursor wave in AD1 aluminum at normal and elevated temperatures. Data from ref. [17].

Figure 8. Rate sensitivity of the flow stress in aluminum at 20°C and 600°C temperatures .

In Fig. 7, the decays of elastic precursor waves in aluminum at normal and elevated temperatures are compared. Extrapolation to smaller distances points on intersection at $h \approx 10$ μm. It may be expected even intuitively that ultimate shear strength should decrease with heating and, as a result, smooth decay in preheated material should start from lower HEL value. Extrapolation of high-temperature dependence $\tau(\dot{\gamma}_p)$ to lower strain rates in Fig. 8 indicates intersection with low-rate branch at strain rate of order of 10^2 s^{-1}. The Hopkinson bar tests do not reveal anomalous thermal hardening at such strain rate, but these tests do not allow measure initial yield stress at zero plastic strain.

Figure 9 compares yield strength data for the Ti-6-22-22S alloy, commercial grade titanium, and titanium of 99.99% purity. The flow stress in the latter makes an essential contribution to the drag of the dislocations. In contrast to pure metals, alloys contain numerous obstacles such as inter-phase boundaries, inclusions, etc. The stress needed to overcome these obstacles far exceeds the forces of phonon drag, which are, therefore, unable to make a significant contribution into the resistance of the alloys to plastic flow. Hardening of a material shifts the transition in drag controlling mechanism towards higher strain rates.

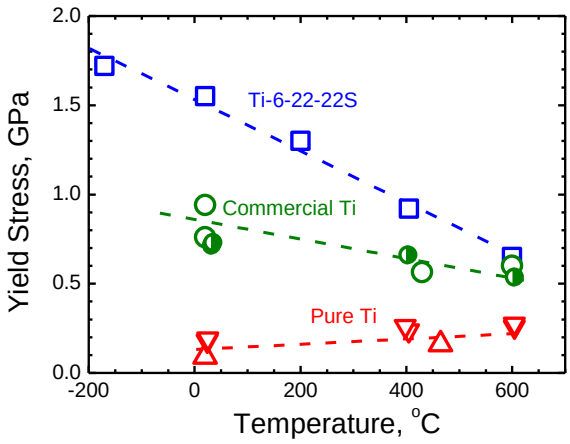

Figure 9. Temperature dependences of dynamic yield stress of titanium and its alloy [9, 25, 26].

Appearance of anomalous growth of HEL with heating correlates with the rate of its decay: it was observed in aluminum and silver where the decay exponent $\alpha \geq 0.5$ and was not observed in alloys where the decay occurs at $\alpha << 0.5$.

Spall fracture

Many measurements of the spall strength [10, 11] have been done for technical materials with a goal to characterize their ability to withstand a high-velocity impacts. On the other hand, the shock wave tests can give also new information about the ultimate strength of materials, kinetics and mechanisms of a damage nucleation and development, topology and statistics of the damage nucleation sites and can be useful in the field of material science. Because of that, investigations of last years are more concentrated on studying the correlations between the structure of materials and their resistance to spall fracture over a wide range of the strain rates and temperatures. Figure 10 summarizes the spall strength data [12, 17, 27-29] for aluminum. The results of the molecular dynamics simulation of spallation [30, 31] and the *ab initio* calculation of the ideal strength [32] are also shown. The resistance to spall fracture of single crystals exceeds that of polycrystalline aluminum and aluminum alloys. Polycrystalline materials contain relatively coarse stress concentrators, such as grain boundaries, inclusions, etc. These defects reduce the stress threshold that initiates damage on them. Obviously, the high dynamic tensile strength of single crystals is a result of their high homogeneity. The extrapolation to the region of higher strain rates is in agreement with the molecular dynamics calculations and predicts the achievement of the ideal strength at a tension rate of about 2×10^{10} s^{-1}.

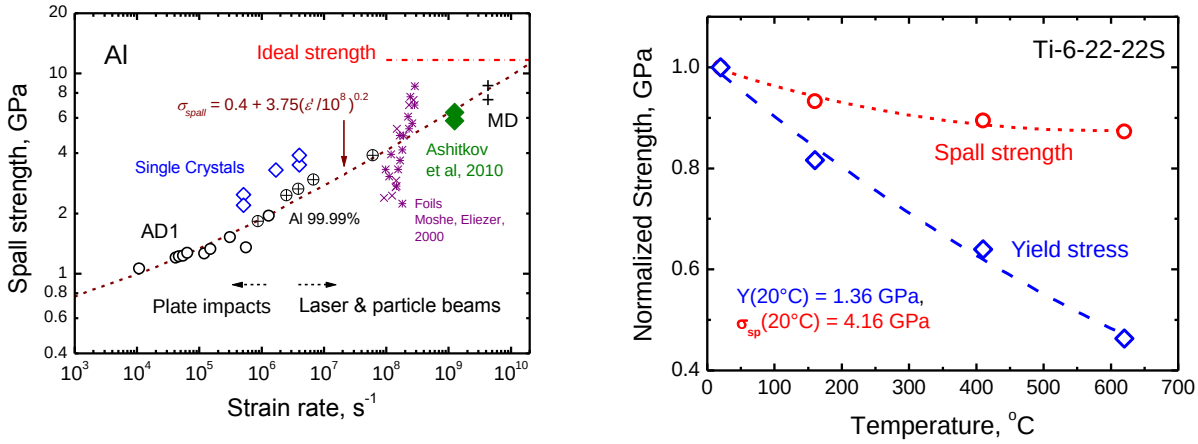

Figure 10. Measured spall strength of aluminum in comparison with the data for different kinds of aluminum. MD indicates results of the molecular dynamics simulation, "Ideal strength" is a result of *ab initio* calculation.

Figure 11. Normalized dynamic yield stress and the spall strength as functions of the temperature for Ti-6-22-22S alloy [33].

Growth of temperature causes decrease of spall strength. For both polycrystalline metals and single crystals, decrease of their dynamic tensile strength with heating up to ~$0.9T_m$ is less than that observed under low-rate tension. With further heating polycrystalline metals lose their spall strength as the melting point T_m is approached, while single crystals retain their high tensile strength even upon traversing the phase boundary of melting in the negative-pressure domain. In the case of

alloys, fast decrease of spall strength begins at lower temperature and spall strength drops to zero with approaching the solidus temperature.

There is no direct correlation between the HEL or yield stress and the spall strength. Figure 11 shows the relative decrease in the yield strength in the plate impact tests much exceeds the spall strength decrease. According to existing models, the initial phase of a high-rate fracture process includes nucleation and growth of numerous pores or cracks. The resistance to growth of voids is controlled by the flow stress in the surrounding matter [10]. Consequently, a rapid decrease of the yield strength with heating should be accompanied by a proportional decrease in the spall strength. Since the observed ratio of the spall strength to the dynamic yield strength is not constant but increases with the temperature, we have to conclude that the spall strength is determined more by the rate of void nucleation rather than their growth.

Coming back to dependence of the spall strength on the material structure, it is interesting that decrease of the grain size by means of severe plastic deformation may cause increase of spall strength [20]. This probably means that the damage nucleation sites in polycrystalline metals are not grain boundaries as themselves but rather impurities concentrated on them.

Behavior of hard brittle material under shock wave loading

Mechanical behaviors of brittle materials, either static or dynamic, are often dominated by fracture under compression in the presence of confining stresses. At low-stress or no confinement, brittle materials loose their load carrying capacity (shear strength) by axial cracking at some threshold stress (failure threshold). Increasing levels of confining stresses tend to suppress axial cracking, increase the failure threshold to higher stress values, and generates brittle to ductile transition in materials. Here we present some recent data on the behavior of ceramics and hard homogeneous materials – sapphire single crystals and glasses.

Ceramics

Figures 12 and 13 present examples of the waveforms recorded in shock-wave experiments with alumina and SiC ceramic samples of various density and thickness. The Hugoniot elastic limit of ceramic material grows with increasing the density: for Al2O3 – from 5 GPa at 3.45 g/cm^3 to 12 GPa at 3.95 g/cm^3. The spall strength of ceramic materials usually is very small and varies within a range of 0.5 – 1.0 GPa.

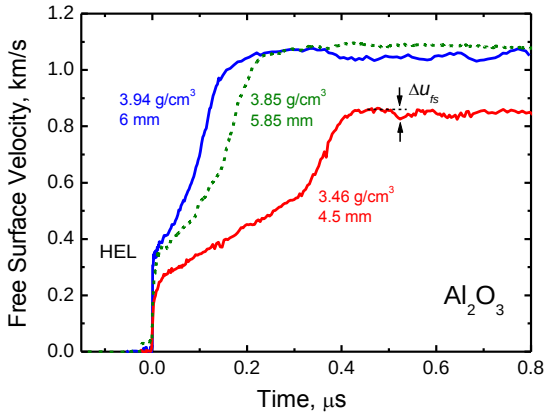

Figure 12. The free surface velocity histories of alumina ceramic samples of various density impacted by 2-mm aluminum flyer plates at 1.8 km/s impact velocity.

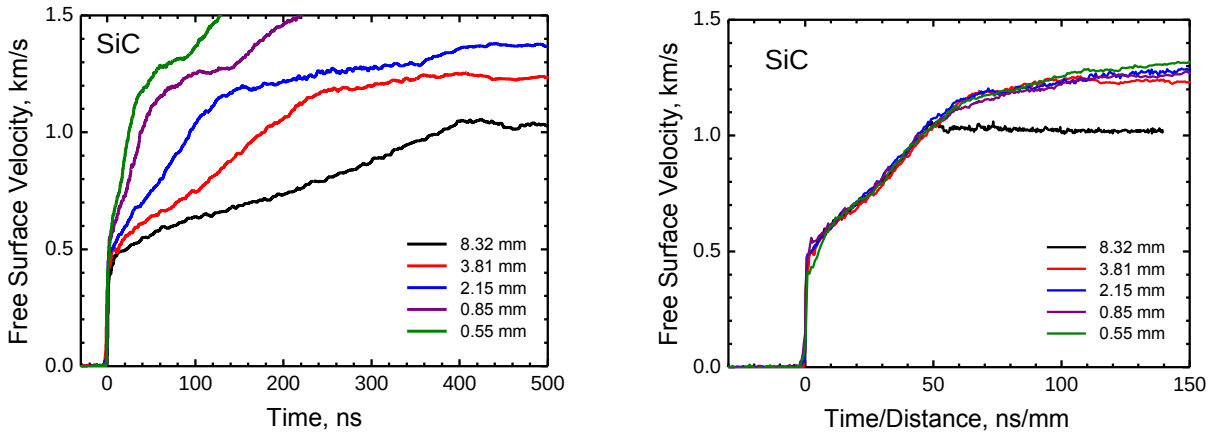

Figure 13. Waveforms recorded for SiC ceramic samples of different thickness in usual and normalized time scale.

The rise of parameters behind the elastic shock is caused by the work hardening rather than by the stress relaxation. It follows from measurements of the wave evolution shown in Fig. 13: self-similar waveforms usually are not observed in relaxing materials. It has been shown by experiments with pre-stressed samples [35] the alumina behaves as ductile material under conditions of the uniaxial shock compression.

Sapphire

Figure 14 presents the waveforms measured for *c*-cut sapphire samples [36]. The particle velocity histories are "noisy" and their reproducibility is low that obviously are a consequence of intrinsic heterogeneity of inelastic deformation. The rise time of the second compression wave is around 150 ns. Also shown in Fig. 14 is a computer simulation of the shock response of a *c*-cut crystal assuming an idealized elastic-plastic strength model and both a high and zero tensile strength. Comparison of measured and computed velocities on release at late times indicates negligible tensile strength after deformation in the plastic wave.

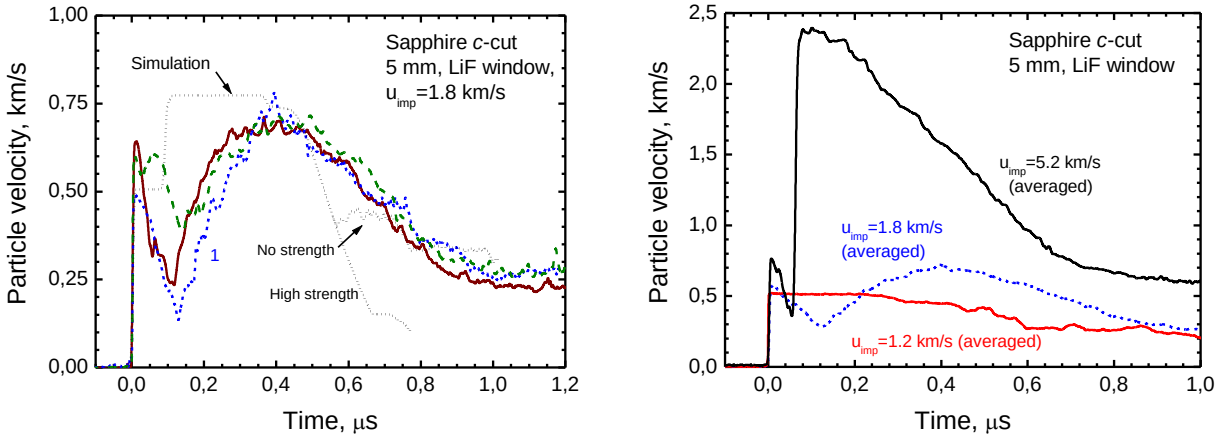

Figure 14. Results of three experiments with *c*-cut sapphire samples at 1.8±0.05 km/s impact velocity.

Figure 15. Averaged particle velocity histories of 5 mm-thick *c*-cut sapphire samples at different impact stresses.

The precursor waveforms with spikes are associated with accelerating stress relaxation behind the precursor front [8].The deep valley behind the elastic spike is only observed at the interface with the low-impedance LiF window if the spall strength of *c*-cut sapphire in the state between the elastic and plastic waves is 2–2.5 GPa or larger. Since sapphire looses its strength after inelastic deformation, the spike-like precursor wave is obviously associated with purely elastic deformation in both compression and unloading.

Figure 15 summarizes experimental data for *c*-cut sapphire samples at three different impact stresses. The waveforms shown are averaged data of two shots at an impact velocity of 1.2 km/s, three shots at 1.8 km/s and two shots at 5.2 km/s. The particle velocity histories measured at highest peak stress are less noisy compared to those recorded at lower impact stresses and are more reproducible. An important aspect of the leading parts of the waveforms is their intersection between elastic and plastic fronts. At intermediate peak value of the stress its relaxation occurs deeper than at low peak stress. Such evolution of the waveforms is unusual; as a rule waveforms vary monotonically with increasing peak stress.

In order to verify the state of sapphire between the elastic and plastic waves we performed additional experiments aimed at determining spall strength at various peak stresses and load durations. Figure 16 shows particle velocity histories recorded at the interface between a 5 mm-thick *c*-cut sample and a water window. The samples were placed on 2 mm-thick aluminum base plates, which were impacted by aluminum flyer plates 0.4 mm or 0.85 mm thick at 1.55 km/s. It can be seen that the waveforms are smooth in their initial parts, but the irregular oscillations appear immediately when fracture begins. In the shot with the thin flyer plate, the peak compressive stress near the sample-window interface was 18.2 GPa. In this shot sapphire demonstrated a spall strength as high as 8.9 GPa. In shot 2 with a larger pulse duration, the peak compressive stress was 20.6 GPa and the spall strength was 4.2 GPa. It was found (shot 3 in Fig. 16) at ~40 ns load duration and 23 GPa peak stress in elastic compression wave the spall strength exceeds 20 GPa. An increase of compressive stress up to 24 GPa in shot 4 and some increase of the total load duration resulted in spallation at a factor of two less tensile stress – 10.4 GPa. Thus, at shock compression below the HEL, sapphire demonstrates the highest values of spall strength, which grow with shortening of the load duration. There is also a trend for the spall strength to decrease with increasing peak compressive stress in the range of the HEL.

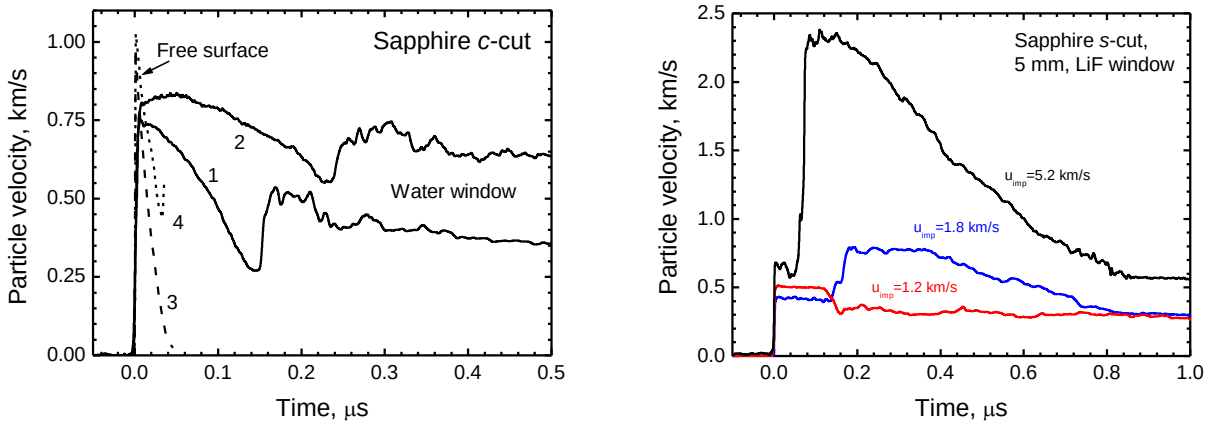

Figure 16. Results of spall tests. 1, 2 are the velocity histories of interfaces between water windows and *c*-cut samples impacted by flyer plates 0.4 mm (curve 1) or 0.85 mm (curve 2) in thickness at 1.55 km/s. 3, 4 are free surface velocity histories of shock loading generated by the ion beam [37].

Figure 17. Results of experiments with s-cut sapphire.

Figure 17 presents results of experiments with *s*-cut sapphire. The step-like structure of the recorded plastic wave is a result of multiple reflections of the elastic-precursor wave between the LiF window and the plastic wave. Accounting for this distortion real rise time in the plastic wave is estimated as 11–12 ns. There still are some irregular oscillations in the waveforms but they are of higher frequencies and lower amplitudes than those recorded in experiments with other orientations. A small rise time and high-frequency "noise" may be considered as evidence of high homogeneity of deformation of *s*-cut sapphire under shock compression. The speed of second (plastic) wave is 8.3 km/s, which is in reasonable agreement with the bulk modulus of sapphire.

Possible mechanisms of plastic deformation of sapphire which are discussed in literature include basal slip, pyramidal slip, prism slip, basal twinning, and rhombohedral twinning. The basal twins and dislocations have the lowest critical resolved shear stress to activation. Experimental data in Table 1 show the HEL values vary from 12.4 GPa up to 24.2 GPa depending on the load direction and the peak stress. The highest HEL values are observed at shock compression perpendicular and parallel to the crystal base plane in experiments with *c*-cut and *m*-cut samples. Uniaxial compression in these directions excludes generation of shear stresses on the basal plane and, correspondingly, activation and movement of dislocations and twins in this plane. Shock compression along the *c*-axis also excludes prism slip. The shape of the waveforms recorded for *s*-cut and *m*-cut sapphire, as compared to data for other load directions, suggests with high probability of the highest contributions of more homogeneous dislocation mechanisms to plasticity in these cases. Irregular oscillations of stress often accompany twinning. Twins can grow with extremely high speed. The unexpected and unusual decrease of recorded HEL values with increasing impact velocity from 1.2 km/s to 1.8 km/s is probably explained by the fact that nucleation of twins requires much higher stresses than their growth.

Failure waves in shock-compressed glasses

The impact loading of a glass and, probably, other brittle materials can result in the appearance of a failure wave. The failure waves present a mode of catastrophic fracture in elastically compressed media that is not limited to impact events. It is regular self-propagating process. One may hope that the investigations of failure waves provide information about the mechanisms and general rules of nucleation, growth, and interaction of the multiple cracks under compression. The term "failure wave" has been introduced in sixtieths [38, 39] when a detonation-like model of fracture of stressed brittle materials was developed. The model supposes an ability of fragmentation occurring within relatively thin layer which propagates through undamaged material with the sound speed. The first theoretical models did not provide a base for correct estimations of kinematical parameters of the failure waves. A similar fracture mode under compression was revealed in shock-wave experiments.

Figure 18 presents the waveforms for K8 crown glass which were measured at two different impact velocities [40]. The rise time of compression wave gradually increases with the increase of the propagation distance that is a result of anomalous compressibility of the glass below its elastic limit and the stress relaxation above it. The waveforms do not exhibit a distinct transition from the elastic to plastic response. Spallation was not observed in these shots, which means that the spall strength of the glass exceeds 6.8 GPa below the HEL and remains very high above it. For comparison, the static tensile strength of glasses is around 0.1 GPa. The reason for such a large discrepancy is that the fracture nucleation sites in homogeneous glass are concentrated on the surface. These incipient microcracks determine the strength magnitude in the static measurements, whereas spall strength is an intrinsic property of matter.

Most of silicate glasses have anomalous longitudinal compressibility within the region of elastic compression where the longitudinal sound speed decreases as the compressive stress

increases that, in turn, causes broadening of the elastic compression wave with its propagation. As a result of an anomalous behavior of longitudinal sound speed, a rarefaction shock wave should be formed in glass at unloading from shock-compressed state if the compression is completely reversible. Since the reversibility of stress−strain processes is a main attribute of elastic deformations, observation of the rarefaction shock (demonstrated by the waveform 2 in Fig. 19) may be considered as evidence of an elastic regime of deformation. Above the HEL the unloading wave speed becomes greater than the compression wave speed that is demonstrated by the waveform 1 in Fig. 19.

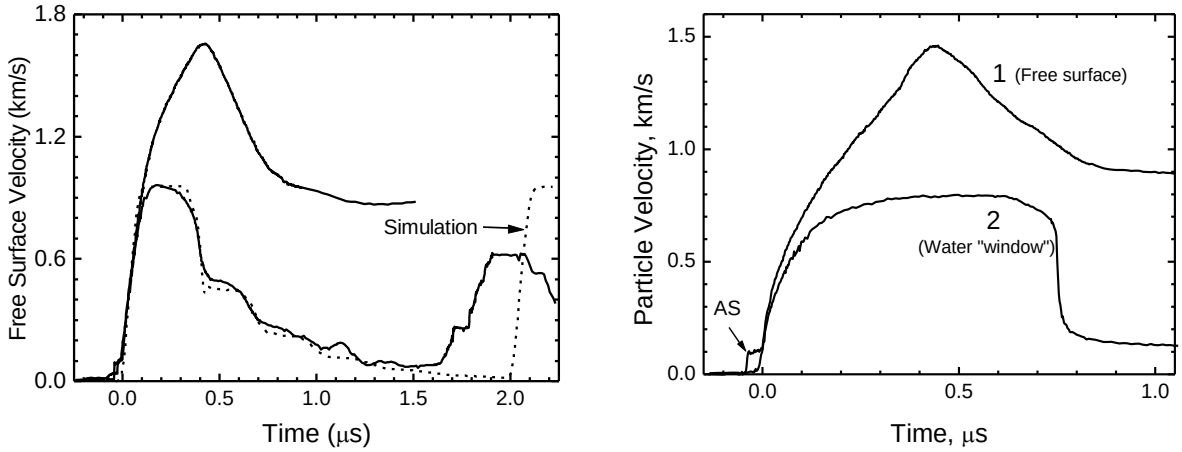

Figure 18. The free surface velocity histories of the K8 crown glass samples at different peak stresses [40]. The dashed line shows results of computer simulations.

Figure 19. Particle velocity histories of soda lime glass plates of thickness 5.9 mm [41]. The wave profile 1 corresponds to impact by aluminum flyer plate 2 mm thick backed by paraffin, with the impact velocity being 1.90±0.05 km/s. The wave profile 2 corresponds to impact by aluminum flyer plate of 2.1 mm thick at the impact velocity 0.97±0.03 km/s, measured through a water window.

In the Fig. 18 the results of the measurements are compared with the computer simulation for the shot of K8 glass target impacted by a low-velocity steel plate. Simulation has been done supposing purely elastic behavior for the glass, and without fracture under both compression and tension. Whereas the computed first velocity pulse is in a reasonable agreement with the measured one, the second velocity pulse arrives at the rear surface later as compared to the measurements. This difference means that the observed second velocity pulse is actually a reflection of the rarefaction wave from a near-surface layer which is not able to sustain tension. In other words, the layer of glass near the impact surface has been failed to the moment when the reflected tensile pulse reached it. Expansion of the cracked layer from the impact surface has been treated as propagation of the failure wave. No any evidences of cracking were observed at peak stress above the HEL.

Figure 20 presents the measured free surface velocity histories of soda lime glass plates at various stress levels where the time is normalized by the sample plate thickness. The wave profiles contain small recompression pulses which are due to the wave reflection from a failed region inside the sample. It follows from consideration of the time−distance diagram shown in Fig. 21 that the failure wave speed c_f may be determined by means of measurement of the time interval t_r between the arrivals of the initial compression wave and the recompression pulse front at the plate free surface. For constant speed of the failure wave the ratio t_r/δ, where δ is the glass plate thickness, should not depend on the plate thickness. As it is seen in Fig. 20, the failure waves propagate at a

constant speed which decreases from 1.58±0.06 km/s at 6.3 GPa of compressive stress to 1.35±0.06 km/s at 4 GPa. Comparison of the time t_r of arrival of re-reflected pulses in Figures 18 and 20 shows that the reflected signal arrives later in the case of short loading pulse. The latter observation indicates that the unloading decreases the failure wave velocity or even arrests the failure wave propagation.

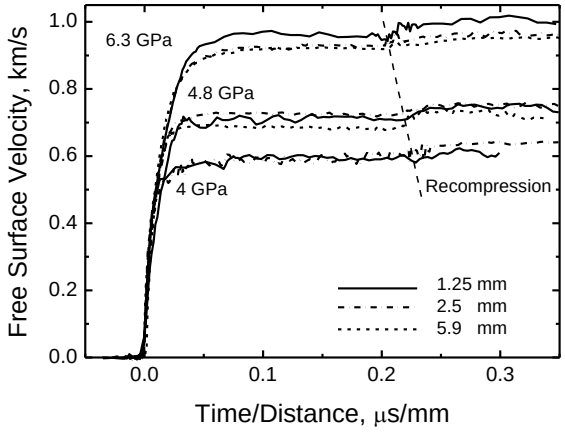

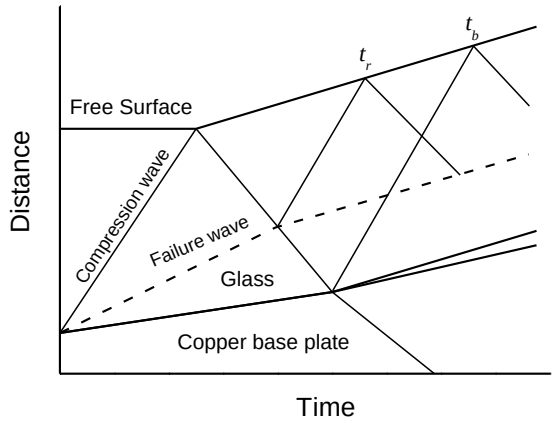

Figure 20. Free surface velocity histories of the soda lime glass plates of different thicknesses at three different stress levels of shock compression [42].

Figure 21. Distance-time diagram of experiments shown in Fig. 20.

Experiments with layered glass samples [41] have shown that the network of growing microcracks in shock-compressed glass may indeed be considered as a wave with a small stress increment which obeys the Rankine-Hugoniot conservation laws. The estimated final state behind the failure wave agrees with direct measurements of the principal stress difference. Kinematics of the failure waves differs from those of elastic−plastic waves. The shock compression wave in an elastic−plastic body becomes unstable at sudden decrease of longitudinal compressibility that occurs when yielding begins. As a result, the wave splits into an elastic precursor wave and a plastic shock wave. The peak stress behind the elastic precursor front is determined by the yield stress. The propagation velocities of the elastic precursor wave front and the second compression wave are determined by the longitudinal and bulk compressibility, respectively. In contrast to that, the propagation velocity of the failure wave is determined by the crack growth speed, which is not directly related to the compressibility.

Since the failure wave nucleates on the glass surface, the magnitude of the leading elastic wave in the shocked specimen consisting of layered glass plates should decrease as a result of its decomposition into two waves at each interface. The decrease of elastic wave amplitude repeats at each interface until the failure threshold is reached. Hence, for a sufficiently large number of layered glass plates, an elastic precursor wave with its amplitude close to the failure threshold could be formed. Figure 22 presents results of two shots where free surface velocity histories were recorded for one thick glass plate and layered assemble of 8 thin glass plates, subjected to the same impact loading. The shot with a pile shows the waveform that is typical for elastic−plastic solids. The final magnitude of the free surface velocity is practically equal to that of a single glass plate. The response of a layered assembly of thin brittle plates as compared to that of one thick plate is a simple way to diagnose nucleation of the failure process on the plate surfaces and determine the failure threshold.

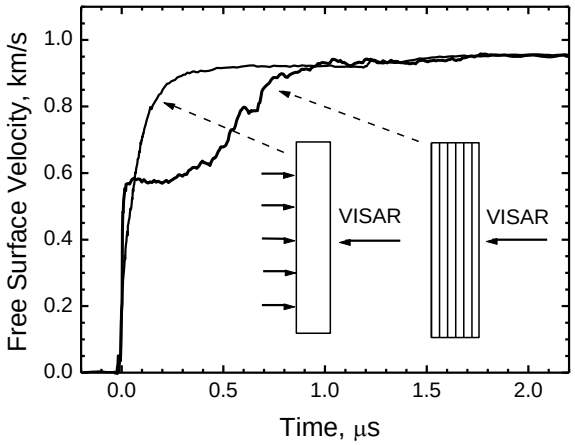

Figure 22. The free surface velocity histories recorded in two shots with layered assemblies of 8 soda lime glass plates of 1.2 mm average thickness in comparison with the data for single glass plate 5.9 mm thick.

Summary

The significance of investigations into the inelastic deformation and fracture of solids under shock-wave loading is due both to the unique opportunity of investigating the area of strength and plasticity physics for the highest and reliably measured rates of straining and to diverse practical demands, which are not limited only to shock actions. Shock-wave experiments enable obtaining information about the most basic strength properties of materials under conditions which eliminate the surface effect on the deformation and fracture. In this way, it is possible to realize the states of solids which are close to the maximum possible strength and thereby estimate their strength resource experimentally. The first investigations into the elastic-plastic and strength properties of metals and alloys at elevated temperatures and extremely high rates of shock-wave loading revealed interesting effects, which might have been expected but had nevertheless not been predicted by the theory. The results of measurements show that the effect of temperature on the yield stress may be opposite to what takes place at low and moderate rates of straining.

The last decade has seen the rise of interest in the behavior of brittle materials. In particular, active studies are being made of failure waves. Failure wave generation is one of the mechanisms responsible for the catastrophic loss of strength of highly consistent brittle materials and exemplifies a nonlocal reaction of a material to loading. The set of techniques for diagnosing the states of shock-compressed brittle materials has been substantially broadened by the development of a methodology for testing pre-stressed specimens and testing with diverging shock waves. In the coming decade one would expect a substantial broadening of the application of shock-wave techniques for solutions to the problems of material science and strength and plasticity physics. Further investigations of strength variations at the mesolevel and elucidation of the formation mechanism of localized shear bands will facilitate the development of new high-strength materials and the improvement of their processing technology. Elucidating the details of the mechanism of brittle fracture under compression would foster advances in the design and application of superhard materials and in earthquake prognostication.

Acknowledgement

Financial support from Russian Foundation for Basic Research via the Grants No 11-02-01141-a and 11-08-12107-ofi-m-2011 is gratefully acknowledged.

References

[1] Clifton, R.J., Appl. Mech. Rev. **43**, S9 (1990)
[2] Meyers, M.A., Benson, D.J., Vohringer, O. et al., Mater. Sci. Eng., A **322**, 194 (2002).
[3] Al'shitz, V.I. and Indenbom, V.L., Sov. Phys. – Usp. **18**, 1 (1975).
[4] Duvall, G.E. In: Strss Waves in Anelastic Solids, edited by H. Kolsky and W. Prager, p. 20, Springer-Verlag, Berlin, 1964
[5] Asay, J.R., Fowles, G.R., and Gupta, Y., J. Appl. Phys. **43**, 744 (1972).
[6] Chhabildas, L.C. and Asay, J.R., J. Appl. Phys., **50**, 2749 (1979).
[7] Swegle, J.W. and Grady, D.E., J. Appl. Phys. **58**, 692 (1985)
[8] Kanel, G.I., Razorenov, S.V., Fortov, V.E., Shock-Wave Phenomena and the Properties of Condensed Matter. Springer, New York, 2004
[9] Kanel, G.I., Razorenov, S.V., and Fortov, V.E., J. Phys. – Condens. Mat., **16**, S1007 (2004)
[10] Antoun, T., Seaman, L., Curran, D.R., Kanel, G.I., Razorenov, S.V., and Utkin, A.V., Spall Fracture. Springer, New York, 2003.
[11] Kanel, G. I., Int. J. Fract., **163**, 173 (2010)
[12] Ashitkov, S.I., Agranat, M.B., Kanel, G.I., Komarov, P.S., Fortov, V.E., JETP Letters, **92**, 516 (2010)
[13] Whitley, V.H., McGrane, S.D., Eakins, D.E., Bolme, C.A., Moore, D.S., and Bingert, J.F., J. Appl. Phys., **109**, 013505 (2011)
[14] Ashitkov, S.I., Agranat, M.B., Kanel, G.I., and Fortov, V.E. In: Shock Compression of Condensed Matter 2011, Eds: M.L. Elert, Wi.T. Buttler, J.P. Borg, J.L. Jordan, T.J. Vogler. AIP Conf. Proc., 1426, pp. 953-956 (2012)
[15] Gupta, Y.M., Winey, J.M., Trivedi, P.B., et al., J. Appl. Phys. **105**, 036107 (2009).
[16] Winey, J.M., LaLone, B.M., Trivedi, P.B., et al., J. Appl. Phys. **106**, 073508 (2009).
[17] Garkushin, G.V., Kanel, G.I., and Razorenov, S.V., Phys. Solid State **52**, 2369 (2010).
[18] Arvidsson, T.E., Gupta, Y.M., and Duvall, G.E. J. Appl. Phys. **46**, 4474 (1975).
[19] Sakino, K. J. Phys. IV France, **10**, Pr9-57 (2000).
[20] Garkushin, G.V., Ignatova, O.N., Kanel, G.I., Meyer, L., Razorenov, S.V., Mech. Solids, **45**, 624 (2010)
[21] Razorenov, S.V., Kanel, G.I., Garkushin, G.V., Ignatova, O.N. Phys. Solid State, 54(4), 790-797 (2012)
[22] Olmsted, D.L., Hecto, G., Curtin, W.A. and Clifton, R.J., Modelling Simul. Mater. Sci. Eng. **13**, 371 (2005)
[23] Kuksin, A.Yu., Norman, G.E., Stegailov, V.V., and Yanilkin, A.V., J. Eng.Thermophys., **18,** 197 (2009).
[24] Garkushin, G.V., Kanel, G.I. and Razorenov, S.V. In: Shock Compression of Condensed Matter 2011, Eds: M.L. Elert, Wi.T. Buttler, J.P. Borg, J.L. Jordan, T.J. Vogler. AIP Conf. Proc., 1426, pp. 935-938 (2012)
[25] Kanel, G.I., Razorenov, S.V., Zaretsky, E.B., Herrman, B., and Meyer, L., Phys. Solid State **45**, 656 (2003).
[26] Zaretsky, E.B., J. Appl. Phys. **104**, 123505 (2008)
[27] Kanel, G.I., Razorenov, S.V., Bogatch, A.A., Utkin, A.V., Fortov, V.E., and Grady, D.E.. J. Appl. Phys., **79**, 8310 (1996).
[28] Kanel, G.I., Razorenov, S.V., Baumung, K., and Singer, J., J. Appl. Phys. **90**, 136 (2001).
[29] Eliezer, S., Moshe, E., and Eliezer, D., Laser and Particle Beams **20**, 87 (2002)
[30] Zhakhovskii, V.V., Inogamov, N.A., Petrov, Yu.V. et al., Appl. Surf. Sci. **255**, 9592 (2009)
[31] Zhilyaev, P.A.,, Kuksin, A.Yu., Stegailov, V.V., Yanilkin, A.V., Phys. Solid State, **52**, 1619 (2010)
[32] Sin'ko, G.V. and Smirnov, N.A., JETP Lett. **75**, 184 (2002).
[33] Krüger, L., Meyer, L., Razorenov, S.V., Kanel, G.I., Int. J. Impact Eng., **28**, 877 (2003)
[34] Zaretsky, E.B., Kanel, G.I. J. Appl. Phys. **110** (7), 073502 (2011)
[35] G.I. Kanel, E.B. Zaretsky, A.Rajendran, S.V. Razorenov, A.S. Savinykh, V. Paris. Int. J. Plasticity **25**(4) 649–670 (2009)
[36] G.I. Kanel, W.J. Nellis, A.S. Savinykh, S.V. Razorenov, and A.M. Rajendran. J. Appl. Phys. **106**, 043524 (2009)
[37] G.I.Kanel, S.V.Razorenov, A.V.Utkin, K.Baumung, H.U.Karov, and V.Licht, in High-Pressure Science and Technology - 1993. edited by S. C. Schmidt et al (American Inst of Physics, NY), 1043 (1994).
[38] Galin L.A. and Cherepanov G.I. *Dokl. AN SSSR*, **167**(3), 543 (1966). (In Russian).
[39] Grigoryan S.S. *Mekhanika Tverdogo Tela*, 1977, no 1, 173; Slepyan L.I., ibid, 181 (In Russian).
[40] Kanel G.I., Razorenov S.V., Utkin A.V., Hongliang He, Fuqian Jing, and Xiaogang Jin. *High Pressure Research*, **16**, 27 (1998).
[41] Kanel G.I., Bogatch A.A., Razorenov S.V., Zhen Chen. *J. Appl. Phys.*, **92**(9), 5045 (2002).
[42] Kanel G.I., Bogach A.A., Razorenov S.V., Savinykh A.S., Chen Z., and Rajendran A. A. In: Shock Compression of Condensed Matter – 2003, Eds. M. D. Furnish et al., AIP CP **706**, pp. 739 (2004).